

Dominance of correlation and relativistic effects on photodetachment time delay well above threshold

Soumyajit Saha,¹ Pranawa C. Deshmukh,^{2,3} Anatoli S. Kheifets,⁴ and Steven T. Manson⁵

¹ *Department of Physics, Indian Institute of Technology Madras, Chennai 600036, India*

² *Department of Physics, Indian Institute of Technology Tirupati, Tirupati, 517506, India*

³ *Department of Physics, Indian Institute of Science Education and Research Tirupati, Tirupati, 517507, India*

⁴ *Research School of Physics and Engineering, The Australian National University, Canberra ACT 2601, Australia*

⁵ *Department of Physics and Astronomy, Georgia State University, Atlanta, 30303, USA*

(Dated: September 20, 2018)

Wigner time delay in photodetachment from the $3p_{3/2}$ and $3p_{1/2}$ subshells of Cl^- have been studied in the vicinity of the $2p_{3/2}$ and $2p_{1/2}$ thresholds, using the relativistic random phase approximation (RRPA). The results show time delay spectra dominated by many-body correlations along with very complicated dependence on the energy over a broad spectral range. In addition, the time delay spectra of the two spin-orbit split $3p$ subshells differ significantly from one another, thereby revealing the importance of relativistic effects even in the case of a low- Z system.

PACS numbers: 32.80.Rm 32.80.Fb 42.50.Hz

Probing Wigner time delay [1–3] in photoemission unearths the motion of electrons in transition in the real time domain, i.e., at the attosecond level. Modern studies of photoemission time delay have been triggered by pioneering experiments on the Ne [4] and Ar [5] atoms that opened a new avenue to explore the ultrafast electron dynamics of atomic and molecular (and condensed matter) systems, and led to a plethora of recent theoretical and experimental studies of time delay over a broad range of systems. Much of this work is reviewed in [6], and [7–24] provide a representative selection of more recent investigations. Aside from the interest in time delay as an indicator of electron transition dynamics on the attosecond time scale, since the time delay is related to the energy derivative of the phase of the transition matrix element [1–3], it also provides information on the most elusive part of it, the phase; the magnitude can be obtained much more easily from the respective cross sections.

In general, it had been seen that, in almost all the cases, the time delay for the photoionization of a given atomic or molecular subshell approaches zero with increasing photoelectron kinetic energy [6–8]. However, it is known that outer-shell photoionization is affected by correlation in the vicinity of inner-shell thresholds; this aspect of correlation is known as interchannel coupling and its effects have been seen in photoionization cross sections and angular distributions both theoretically and experimentally; see [25] and references therein. Very recently, it was shown that these interchannel coupling effects extend to time delay significantly as well [21]. Specifically, it was shown that, over a broad range of atoms and energies, the Wigner time delay for outer-shell photoemission that was effectively zero below an inner-shell threshold, experiences a significant jump above the inner-shell threshold, as much as about 30 as. Above the inner threshold, however, the magnitude of time delay was found to decrease monotonically.

These investigations have prompted us to look at time

delay in negative ions whose photoemission is known to be dominated by correlation [26]; also very little is known about photodetachment time delay [27, 28]. In addition, time delay is generally measured using two photons, so that the total time delay, $\tau = \tau_w + \tau_{cc}$, where, τ_w is the Wigner time delay and τ_{cc} is continuum-continuum (coulomb-laser-coupling) correction, a measurement-induced delay due to the electron being probed by the second (laser) photon in a long-range potential with a Coulomb tail of charge Z [27, 29]. Of importance here is that τ_{cc} effectively vanishes when the atomic potential is short-range, as in photodetachment, making the interpretation of experiment much more straightforward [27]. Ar-like Cl^- has been chosen for this study, and we look at $3p$ photodetachment in the vicinity of the $2p$ thresholds; among the reasons for this choice are the closed-shell nature of the ion that facilitates interpretation of the results, and that there are inner shells in an experimentally-convenient region. The results demonstrate: that the interchannel effects on time delay in negative ions are far greater than in neutral atoms; that the energy dependence is far more complex than the simple decreasing behavior of atoms; that relativistic effects play a vital role, even at such low Z ; and that these effects extend over tens of eV.

A relativistic formulation is required to investigate effects due to spin-orbit-splitting of the $2p$ thresholds, and to study the time delay in both the $3p_{3/2}$ and $3p_{1/2}$ subshells individually. The relativistic random phase approximation (RRPA) [30], based on the Dirac equation, and which includes both initial-state correlation and final-state interchannel coupling, is employed for the present calculations, along with our previously-reported theoretical development [15]. Aside from being relativistic *ab initio*, RRPA is gauge-invariant, and it allows the possibility of performing truncated calculations in which certain channels are omitted as a means of pinpointing the specific interchannel coupling responsible for various observable effects. We consider incident photons linearly

TABLE I: Theoretical and experimental [33] photodetachment thresholds of Cl^- in eV.

Subshell(Cl^-)	DF(eV)	Exp.(eV)	Subshell(Cl^-)	DF(eV)
$3p_{3/2}$	4.03	3.62	$3s_{1/2}$	20.13
$3p_{1/2}$	4.17	3.73	$2p_{3/2}$	208.87
			$2p_{1/2}$	210.64
			$2s_{1/2}$	280.22

polarized in the z -direction, and we investigate the time delay, which is angle-dependent in general [23, 31, 32], in the direction parallel to the polarization.

The five possible relativistic transitions from $3p$ subshell are $3p_{1/2} \rightarrow \varepsilon s_{1/2}, \varepsilon d_{3/2}$ and $3p_{3/2} \rightarrow \varepsilon s_{1/2}, \varepsilon d_{3/2}, \varepsilon d_{5/2}$. For a transition from an initial state, $a(ljm)$, to the symmetry allowed final states, $\bar{a}(\bar{l}\bar{j}\bar{m})$, we define the dipole matrix element [15]

$$D_{n\kappa \rightarrow E\bar{\kappa}} = i^{1-\bar{l}} e^{i\delta_{\bar{\kappa}}} \langle \bar{a} \| Q_1^{(1)} \| a \rangle, \quad (1)$$

where,

$$\langle \bar{a} \| Q_1^{(1)} \| a \rangle = (-1)^{j+1/2} [\bar{j}][j] \begin{pmatrix} j & \bar{j} & J \\ -1/2 & 1/2 & 0 \end{pmatrix} \pi(\bar{l}, l, J - \lambda + 1) R^{(1)}(\bar{a}, a) \quad (2)$$

is the (complex) reduced matrix element for an electric dipole transition and $\delta_{\bar{\kappa}}$ is the phase of the continuum wave with $\bar{\kappa} = \mp(\bar{j} + \frac{1}{2})$ for $\bar{j} = (\bar{l} \pm \frac{1}{2})$. The axially symmetric transition amplitudes contributing to the photodetachment process in the polarization z direction are:

$$\begin{aligned} T_{3p_{1/2}} &= +\frac{1}{\sqrt{6}} Y_{00} D_{3p_{1/2} \rightarrow \varepsilon s_{1/2}} + \frac{1}{\sqrt{15}} Y_{20} D_{3p_{1/2} \rightarrow \varepsilon d_{3/2}} \\ T_{3p_{3/2}} &= +\frac{1}{\sqrt{6}} Y_{00} D_{3p_{3/2} \rightarrow \varepsilon s_{1/2}} - \frac{1}{5\sqrt{6}} Y_{20} D_{3p_{3/2} \rightarrow \varepsilon d_{3/2}} \\ &\quad - \frac{1}{5} \sqrt{\frac{3}{2}} Y_{20} D_{3p_{3/2} \rightarrow \varepsilon d_{5/2}}. \end{aligned} \quad (3)$$

Here Y_{lm} are the spherical harmonics evaluated in the direction of polarization, and all of the phase information is contained in the D 's. The Wigner time delay, in atomic units $e = \hbar = m = 1$, is simply the energy derivative of the phase of the amplitude,

$$\tau_{3p_j} = \frac{d}{dE} \tan^{-1} \left[\frac{\text{Im} T_{3p_j}}{\text{Re} T_{3p_j}} \right] \quad (4)$$

Calculations have been performed by coupling all the 14 relativistic dipole channels from the $3p$, $3s$, $2p$ and $2s$ subshells; the $1s$ channels are omitted since the $1s$ threshold is so far away energetically (about 3 keV) that these channels have negligible effect on photoemission in the 210 eV vicinity of the $2p$ thresholds. To emphasize the effects of the inner-shell channels, calculations coupling

only the seven $3p$ and $3s$ channels were also performed. The RRPA uses Dirac-Fock (DF) photoemission threshold energies, given in Table 1 and compared with available experimental thresholds [33].

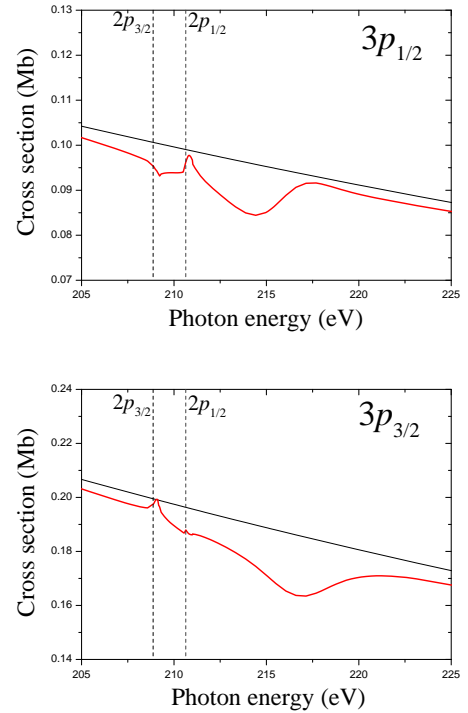


FIG. 1: (color online) Photodetachment cross sections for the $3p_{1/2}$ subshell of Cl^- (upper panel) and the $3p_{3/2}$ subshell (lower panel) in the vicinity of the $2p$ thresholds calculated at the 14-channel (thick red curve) and 7-channel (thin black curve) levels as explained in text. The $2p$ thresholds are indicated by vertical dashed lines.

The results for the cross sections for the two spin-orbit-split $3p$ channels are shown in Fig. 1. Of interest in these results is that there is significant structure in the fully coupled cross sections for both cases in the neighborhood of the $2p$ thresholds, while the 7-channel results are smooth and monotonically decreasing; it is, thus, evident that it is the interchannel coupling of the $3p$ photodetachment channels with the $2p$ that is responsible for the structure. This occurs because the $2p$ cross sections (not shown) are about an order of magnitude larger than the $3p$, in the vicinity of the $2p$ thresholds, so that interchannel coupling between the channels from $3p$ and $2p$ alters the $3p$ photodetachment strength considerably. This phenomenon is known for some time [25, 34]; what is new here is the complicated energy dependence of the perturbed cross sections, and that this is the first indication of the phenomenon in a negative ion. The structure in the $3p$ cross section mirrors the structure in the $2p$ cross sections, in a general sense. Very close to the $2p$ thresholds, the $3p$ cross sections acquire a structure that is characteristic of the $2p \rightarrow \varepsilon s$ channels,

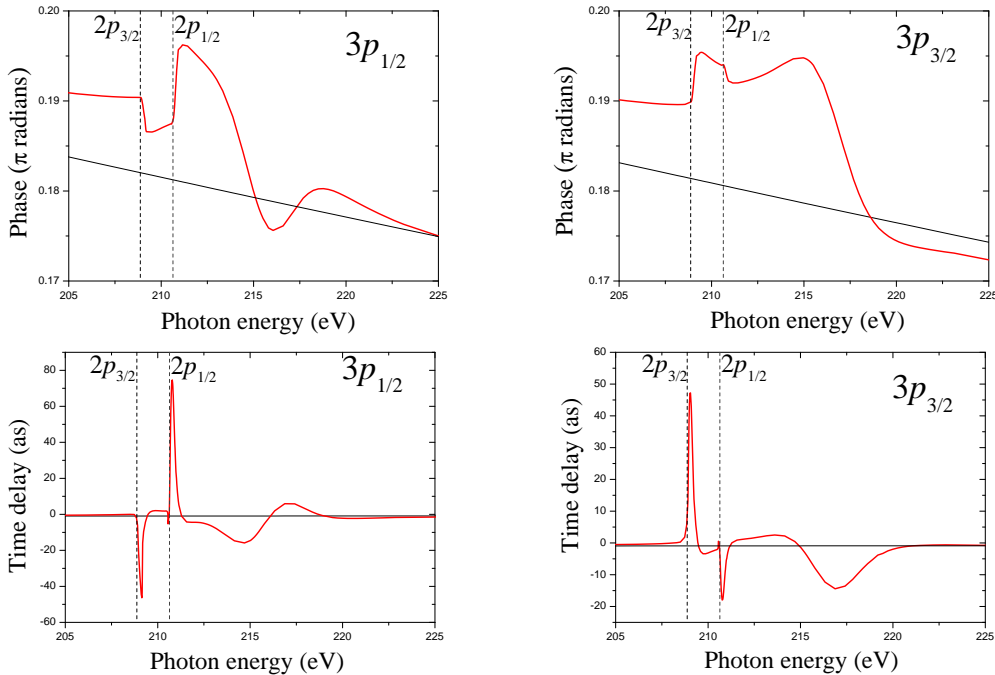


FIG. 2: (color online) Phases of the $3p_{1/2}$ subshell of Cl^- (upper left panel) and the $3p_{3/2}$ subshell (upper right panel) and time delays (lower left and lower right panels, respectively) in the vicinity of the $2p$ thresholds calculated at the 14-channel (thick red curve) and 7-channel (thin black curve) levels as explained in text. The $2p$ thresholds are indicated by vertical dashed lines.

which dominate the $2p$ cross sections near threshold because the centrifugal barrier repels the photoelectron in the d -partial wave. Furthermore, several eV above threshold, the structure acquired by the $3p$ cross sections is characteristic of the $2p \rightarrow \varepsilon d$ shape resonances, produced by the centrifugal potential, which dominate the $2p$ cross sections in this region. Note that the correlated cross section is always below the uncorrelated one, indicating that the contribution of interchannel coupling is of the opposite sign from the unperturbed matrix elements. It is also evident, from Fig. 1, that the structures in the two cross sections are rather different, both between the two $2p$ thresholds, and above, e.g., the dip in the $3p_{1/2}$ cross section occurs at 214 eV, while the dip in the $3p_{3/2}$ cross section is seen at 217 eV. This is a clear indication of relativistic interactions, which is somewhat surprising at such a low Z . Unfortunately, there are no existing experimental results for comparison, in this case, to assess the accuracy of these theoretical predictions.

In any case, it is clear that correlation in the form of interchannel coupling introduces significant structure in the magnitudes of the photoionization amplitudes. It is, thus, likely that the phases are similarly affected. This is exactly what happens, as seen in the upper panels of Fig. 2, where the 7-channel phases are monotonically decreasing, which is a characteristic of the unperturbed phases well above their thresholds, while the perturbed 14-channel phases exhibit considerably complicated structure. This behavior is a significant departure

from the corresponding case in neutral atomic photoionization where the magnitude of the phase induced by interchannel coupling is maximal at the inner-shell threshold, then falls off monotonically with increasing energy [21]. As discussed in connection with the cross sections, very close to the $2p$ thresholds, the phase arises from the interchannel coupling with the $2p \rightarrow \varepsilon s$ channels, while at higher energies, the interaction with the $2p \rightarrow \varepsilon d$ channels, with their associated shape resonances, is the crucial perturbation. It is also noteworthy that the phases of the spin-orbit split $3p$ amplitudes obtained in the 14-channel result are seen to be markedly different from each other (Fig. 2), thus emphasizing that the phases too are strongly affected by relativistic interactions. Without the correlation induced by interchannel coupling, Fig. 2 shows that the two $3p$ phases are essentially the same.

The Wigner time delays generated from the phases, Eq. (4), are shown in the lower panels of Fig. 2 for the $3p_{1/2}$ and $3p_{3/2}$ subshells of Cl^- . The outstanding aspect of these results is a dramatic energy dependence of the time delay spectra, reaching large positive and large negative values over a relatively small energy range, along with the fact that relativistic effects cause the time delays in the two cases to be rather significantly different. The $3p_{1/2}$ time delay is seen to exhibit a large and negative spike, just above the $2p_{3/2}$ threshold, while the $3p_{3/2}$ time delay shows a large and positive spike; and the reverse occurs just above the $2p_{1/2}$ threshold. This can be explained from the lowest order perturbation theory analy-

sis [21] which equates the imaginary part of the inter-shell correlation-induced amplitude to the dipole matrix element of the transition in the inner shell, $2p_{1/2} \rightarrow \epsilon s_{1/2}$ and $2p_{3/2} \rightarrow \epsilon s_{1/2}$ in the present case. From Eq. (2) it can be seen that these matrix elements have opposite signs and differ by a factor of $\sqrt{2}$. At somewhat higher energies, both $3p_{1/2}$ and $3p_{3/2}$ time delays display indications of the interchannel coupling with the $2p \rightarrow \epsilon d$ shape resonances, albeit the manifestation in the two cases is seen to be rather different. This is so because all the dipole matrix elements in the $2p_j \rightarrow \epsilon d_j$ channels have the same sign. Note that the black lines in the lower two panels of Fig. 2 are the 7-channel (i.e., without coupling the $2p$ channels) $3p_{1/2}$ and $3p_{3/2}$ Wigner time delays, *not* the x axis. This demonstrates that all of the phenomenology exhibited in the $3p$ time delays is the result of correlation in the form of interchannel coupling. These results are in sharp contrast to photoionization of the neutral Ar atom (which is isoelectronic to Cl^- , where the time delays are monotonically decreasing in magnitude above the $2p$ thresholds, i.e., they are devoid of any structure. It is, thus, evident, that the effects of multielectron correlation, in the form of interchannel coupling, on the Wigner time delay of an outer-shell photoemission in the neighborhood of inner-shell thresholds for negative ion photodetachment differs markedly, both quantitatively and qualitatively, from photoemission from neutral atoms.

The separation of the $3p_{1/2}$ and $3p_{3/2}$ thresholds is only slightly more than 0.1 eV, so it is unlikely that the individual time delays could be resolved at the present stage of experimental development. Thus, the unresolved (average) $3p$ time delay has been calculated, the $3p_{1/2}$ and $3p_{3/2}$ time delay weighted by their respective cross sections, i.e.,

$$\tau_{3p} = \frac{\tau_{3p_{1/2}} |T_{3p_{1/2}}|^2 + \tau_{3p_{3/2}} |T_{3p_{3/2}}|^2}{|T_{3p_{1/2}}|^2 + |T_{3p_{3/2}}|^2} \quad (5)$$

and the results are shown in Fig. 3. Although some of the physics of the individual subshell time delay is lost in the average, Fig. 3 shows very significant narrow structure immediately above each $2p$ threshold, owing to the $2p \rightarrow \epsilon s$ transitions. The broader structures at somewhat higher energies are traced to the $2p \rightarrow \epsilon d$ shape resonances. The 7-channel result, without the interchannel coupling, is seen to be essentially zero in Fig. 3. It is evident then, that, despite the averaging process inherent in examining only the unresolved time delay, there is still important physics remaining; consequently, this is a very attractive case for experimental investigation.

Furthermore, there is nothing special about the case of Cl^- photodetachment. Cl^- was chosen as a test case because the similar situation in neutral Ar photoemission has been studied [21]. But the effective details in this report should be exhibited generally in the photodetachment time delay of outer shell in the vicinity of inner thresholds, although the details will vary both qualitatively and quantitatively, with each case.

In summary, using the photodetachment of Cl^- as a

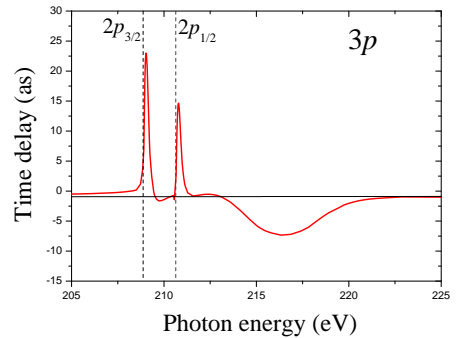


FIG. 3: Wigner time delay of the unresolved $3p$ subshell of Cl^- in the vicinity of the $2p$ thresholds calculated at the 14-channel (thick red curve) and 7-channel (thin black curve) levels as explained in text. The $2p$ thresholds are indicated by vertical dashed lines.

case study, the calculations demonstrate that Wigner time delays of outer-shell photoemission in the vicinity of inner-shell thresholds for negative ions are dominated by many-body correlations in the form of interchannel coupling which give rise to time delays that are quite large and exhibit a very complex energy dependence, much different from the situation for neutral atom photoemission. In addition, relativistic interactions are extremely important, an unexpected result at such low Z . Finally, the results suggest a fruitful area for experimental inquiry. With a recent expansion of attosecond spectroscopy to a broader photon energy range [16, 35], experimental verification of the present results becomes within the reach.

This work is enabled by the infrastructure and support extended to our research group by the Director, Indian Institute of Technology Tirupati, which includes hospitality to SS and STM. This work was supported by the Chemical Sciences, Geosciences, and Biosciences Division, Office of Basic Energy Sciences, Office of Science, US Department of Energy.

-
- [1] E. P. Wigner, Phys. Rev. **98**, 145 (1955).
 - [2] L. E. Eisenbud, Ph. D. thesis, Princeton Univ. (1948).
 - [3] F. T. Smith, Phys. Rev. **118**, 349 (1960).
 - [4] M. Schultze *et al*, Science **328**, 1658 (2010).
 - [5] K. Klünder *et al*, Phys. Rev. Lett. **106**, 143002 (2011).

- [6] R. Pazourek *et al*, Rev. Mod. Phys. **87**, 765 (2015) and references therein.
- [7] T. Barillot *et al*, Phys. Rev. A **91**, 033413 (2015).
- [8] A. S. Kheifets *et al*, Phys. Rev. A **92**, 063422 (2015).
- [9] M. Sabbar *et al*, Phys. Rev. Lett. **115**, 133001 (2015).

- [10] P. Hockett *et al*, J. Phys. B **49**, 095602 (2016).
- [11] M. Huppert *et al*, Phys. Rev. Lett. **117**, 093001 (2016).
- [12] S. Heuser *et al*, Phys. Rev. A **94**, 063409 (2016).
- [13] V. Gruson *et al*, Science **354**, 734 (2016).
- [14] M. Kotur *et al*, Nat. Comm. **7**, 10566 (2016).
- [15] A. S. Kheifets *et al*, Phys. Rev. A **94**, 013423 (2016).
- [16] M. Isinger *et al*, Science **358**, 893 (2017).
- [17] D. A. Keating *et al*, J. Phys. B **50**, 175001 (2017).
- [18] L. Gallmann *et al*, Struct. Dynam. **4**, 061502 (2017).
- [19] M. Fanciulli *et al*, Phys. Rev. Lett. **118**, 067402 (2017).
- [20] C. A Nicolaidis, Appl. Sci. **8**, 533 (2018).
- [21] D. A. Keating *et al* Phys, Rev. A **98**, 013420 (2018).
- [22] P. C. Deshmukh *et al*, J. Phys. B **51**, 065008 (2018).
- [23] C. Cirelli *et al*, Nat. Comm. **9**, 955 (2018).
- [24] J. Vos *et al*, Science **360**, 1326 (2018).
- [25] W. Drube *et al*, J. Phys. B **46**, 245006 (2013).
- [26] S.J. Buckman and C.W. Clark, Rev. Mod. Phys. **66**, 539 (1994) and references therein.
- [27] E. Lindroth and J. M. Dahlström, Phys. Rev. A **96**, 013420 (2017).
- [28] A. S. Kheifets *et al*, Phys. Rev. Lett. **117**, 143202 (2016).
- [29] J. M. Dahlström *et al*, J. Phys. B **45**, 183001 (2012).
- [30] W. R. Johnson and C. D. Lin, Phys. Rev. A **20**, 964 (1979).
- [31] J. Wätzel *et al*, J. Phys. B **48**, 025602 (2015).
- [32] A. Mandal *et al*, Phys. Rev. A **96**, 053407 (2017).
- [33] J. Jose *et al*, Phys. Rev. A **80**, 023405 (2009) and references therein.
- [34] E. W. B. Dias *et al*, Phys. Rev. Lett. **78**, 4553 (1997).
- [35] A. Jain *et al*, Optics Lett. **48**, 4510 (2018).